Atmospheric Research 247 (2021) 105139

Contents lists available at ScienceDirect

Atmospheric Research

journal homepage: www.elsevier.com/locate/atmosres

A new approach to map lightning channels based on low-frequency interferometry

Yanan Zhu[a,*], Michael Stock[b], Phillip Bitzer[a,c]

[a] Earth Systems Science Center, University of Alabama in Huntsville, Huntsville, AL, USA
[b] Earth Networks, Germantown, MD, USA
[c] Department of Atmospheric Science, University of Alabama in Huntsville, Huntsville, AL, USA

ARTICLE INFO

Keywords:
Lightning mapping
Interferometry
Low-frequency

ABSTRACT

A purely interferometric algorithm, named imaging algorithm, has been developed for mapping lightning in the low-frequency band. The imaging algorithm locates a lightning source by computing the three-dimensional correlation of the lightning signals arriving at a pair of lightning sensors, and then summing the correlations of all antenna pairs. This algorithm does not locate the source by solving the non-linear time-of-arrival (TOA) equations, instead the source is located at the global maxima of the total correlation. The lightning map produced by the imaging algorithm for one intracloud flash was compared with that of the hybrid interferometric-TOA algorithm. The imaging algorithm can locate more sources than the hybrid algorithm and produce more complete lightning maps. We also demonstrated that the imaging algorithm can locate multiple concurrent lightning sources even though the recorded signals from the pulses overlap in time at some stations, which is not possible with a traditional TOA-based technique.

1. Introduction

Lightning produces electromagnetic radiation over a wide spectral range, extending from just a few hertz up into the x-ray band. Ground-based systems that locate this lightning emission usually operate in the very low frequency (VLF, 3–30 kHz), low frequency (LF, 30–300 kHz), or very high frequency (VHF, 30–300 MHz) bands. The processes that involve transient high current propagating along a pre-existing channel (e.g. return strokes or K-changes) tend to produce strong emission in the VLF/LF range while the electrical breakdown into virgin air produces strong VHF emission (Cummins and Murphy, 2009). VLF/LF systems are routinely used to locate lightning pulses over regional or even global areas by networks of lightning sensors separated by baselines of hundreds of kilometers, such as U.S. National Lightning Detection Network (NLDN, Cummins et al., 1998) and Earth Networks Total Lightning Network (ENTLN, Zhu et al., 2017). VHF lightning mapping systems offer substantially higher detail over a much smaller area using networks of sensors separated by baselines of a few tens of kilometers (e.g., the Lightning Mapping Array (LMA), Rison et al., 1999; Thomas et al., 2004). In addition to their more limited range, VHF mapping systems have several other limitations. Since the VHF radiation is associated with streamer development (Shi et al., 2019; Hare et al., 2020), VHF measurements cannot be used to determine quantities such as peak current or charge moment for processes in a flash. VHF mapping systems also tend not to locate sources very close to the ground, and so cannot normally be used to determine the ground strike locations of lightning flashes (e.g., Bitzer et al., 2013; Lang et al., 2017). For these reasons, a lightning mapping system which operates at low frequency is desired.

A number of short-baseline, LF lightning locating networks have been developed in the past decade to map lightning in 3D (e.g., Shao et al., 2006; Bitzer et al., 2013; Karunarathne et al., 2013; Lyu et al., 2014; Yoshida et al., 2014; Wang et al., 2016; Shi et al., 2017; Wu et al., 2018). Bitzer et al. (2013) and Yoshida et al. (2014) both used a network of electric field change antennas and located lightning sources using a traditional peak-finding-time-of-arrival (TOA) technique. Three-dimensional maps of lightning were produced, but with fewer and more sporadic sources than the maps produced by an LMA in the VHF band. Lyu et al. (2014) were the first to utilize a hybrid interferometric-TOA algorithm to locate lightning. Here they applied the interferometric cross-correlation techniques used in broadband VHF interferometry (e.g., Sun et al., 2013; Stock et al., 2014; Wang et al., 2020) to the signals recorded by a network of LF magnetic antennas. The maxima of the cross-correlations were used to determine the time difference between pairs of antennas in the array, and then the source was located by solving the non-linear time-difference-of-arrival (TDOA) equations. The

* Corresponding author.
E-mail address: yz0022@uah.edu (Y. Zhu).

https://doi.org/10.1016/j.atmosres.2020.105139
Received 16 April 2020; Received in revised form 3 June 2020; Accepted 15 July 2020
Available online 18 July 2020

advantage of this hybrid processing algorithm is that it can map both discrete and continuous emissions, and thus produce a more complete map of a lightning flash (Lyu et al., 2014). More recently, the Fast Antenna Lightning Mapping Array (FALMA), which also uses a hybrid location technique, has been demonstrated to locate lightning in detail rivaling that of VHF systems including the LMA (Wu et al., 2018, 2019).

In this paper, a purely interferometric algorithm for lightning mapping in the LF is presented. We will refer to this algorithm as the imaging algorithm for simplicity thereafter in this paper since it locates lightning by producing the image of the total correlations for each lightning source. The imaging algorithm was briefly introduced by Stock et al. (2016), but details on the method or performance of the algorithm were omitted. This paper serves to present the imaging algorithm in detail, and compare the lightning maps produced by it with those produced by the hybrid interferometric-TOA technique developed by Zhu et al., (2020). The data used for imaging in this study was obtained from the Córdoba, Argentina Marx Meter Array (CAMMA) during the Remote sensing of Electrification, Lightning, And Mesoscale/microscale Processes with Adaptive Ground Observations (RELAMPAGO) field campaign in Argentina. The CAMMA consists of ten sensors with a typical baseline of 30–60 km. Each sensor is equipped with two (slow and fast) channels for measuring electric field changes produced by lightning at different frequency ranges. The fast channel is much more sensitive than the slow channel and is dedicated to lightning mapping. The lightning maps presented in this paper were produced using the fast channel. The bandwidth for the fast channel is 1.6 kHz to 2.5 MHz with a time decay constant of 100 μs. More detailed information about the CAMMA can be found in Zhu et al. (2020).

2. Location algorithm

The imaging algorithm locates lightning in an entirely different manner than TOA, TDOA, or hybrid-TOA algorithms. Unlike time-of-arrival algorithms, no feature needs to be identified in the recorded signals to locate it. To locate a source, the signals arriving at each pair of antennas are correlated, and then these correlations are projected into a volume containing the source. The source is located at the point of maximum total correlation. The algorithm is similar to the VHF interferometric algorithm presented in Stock and Krehbiel (2014), except that the correlations are projected into a 3D Cartesian volume instead of a 2D cosine plane.

First, a normalized cross-correlation is performed between windowed signals arriving at each pair of stations (i and j). The correlation is a measure of the similarity (correlation coefficient R) between the signals arriving at the stations as a function of lag time ($\Delta t_{i,j}$). As is commonly done, the cross-correlation is normalized by the signal energy term. In this way, two identical signals produce a correlation value of 1 at a lag time of 0. The normalization is not required to locate a source but will give a measure of solution quality in a similar fashion to reduced chi-square seen in TOA algorithms (Thomas et al., 2004). If normalization is omitted, the image amplitude is proportional to the power received by the array.

Next, the correlation of each antenna pair is projected into a volume containing the source. For the windowed emissions produced by a lightning source received by a pair of stations i and j, the correlation at any location $\vec{p}$ in 3D space is defined as.

$$\mathbf{C_{i,j}}(\vec{p}) = \mathbf{R_{i,j}}(\Delta \mathbf{t_{i,j}}(\vec{p})) \tag{1}$$

where $\mathbf{R_{i,j}}$ is the correlation curve (with respect to time lag) from cross-correlation of signals from antennas i and j, and the $\Delta t_{i,j}(\vec{p})$ is the expected lag time for a source at $\vec{p}$ arriving at antennas i and j. The form of $\Delta t_{i,j}(\vec{p})$ depends on the coordinate system that the image is being computed in, for the Cartesian case, $\Delta t_{i,j}(\vec{p})$ is:

$$\Delta t_{i,j}(\vec{p}) = \frac{1}{c}\sqrt{(p_x - i_x)^2 + (p_y - i_y)^2 + (p_z - i_z)^2} - \frac{1}{c}\sqrt{(p_x - j_x)^2 + (p_y - j_y)^2 + (p_z - j_z)^2} \tag{2}$$

where (i_x, i_y, i_z) and (j_x, j_y, j_z) are coordinates of antennas i and j, respectively.

Eq. (1) remains valid in all coordinates systems so long as a unique $\Delta t_{i,j}(\vec{p})$ can be found for each point $\vec{p}$ in the volume. The normalized total correlation for the volume, and image of the source, can then be found by summing across the correlations of all antenna pairs.

$$C(\vec{p}) = \frac{1}{M}\sum_{i=1}^{N-1}\sum_{j=i+1}^{N} R_{i,j}(\Delta t_{i,j}(\vec{p})) \tag{3}$$

in which $C(\vec{p})$ is the normalized total correlation at the location $\vec{p}$, N is the number of stations, M = N(N-1)/2 is the number of station pairs, and $R_{i,j}(\Delta t_{i,j}(\vec{p}))$ taken from eq. (1) is the correlation of one pair of signals at the location $\vec{p}$. The $\frac{1}{M}$ on the right side of the equation is for normalizing the total correlation by the number of station pairs. In the case where there is a single radiating source, the location of the source is where the maximum total correlation is found. Because each $R_{i,j}$ is normalized, the $\frac{1}{M}$ term makes the total correlation C also bounded between +/− 1. In TOA-based algorithms, the location is found by minimizing the residuals of the TOA or TDOA equations; in the imaging algorithm, the location is found by maximizing the total correlation between station pairs.

Fig. 1 shows the results of imaging the signals arriving at six CAMMA stations in a 750-μs window. The imaging was done using a 200-m grid in all x, y, and z directions over a 30 km by 30 km by 9 km volume following the procedure outlined above. In total, the image was computed for 1,012,500 voxels. Fig. 1a shows a plan view slice of the volume image, with the slice going through the z-level containing the brightest voxel, indicated with a black dashed line in Fig. 1b. The lightning source is located in the center of the slice at the center of the bright red portion of the image, whose coordinate is [−22 km, −4.6 km, 5.2 km]. The origin of the coordinates used in this paper is CAMMA station 11, which is about the center of the array. Surrounding the central maxima are numerous light blue regions, these are the sidelobes of the interferometric image. In far-field broadband interferometry, the side-lobes show up as lines emanating from the bright source (Stock and Krehbiel, 2014). Here, the source is close enough to the array to be in the near-field (usually a few wavelengths away), and so the side lobes show up as curved lines emanating from the bright source. As the signal-to-noise ratio of the signals recorded at the sensors gets worse, the amplitude of the side-lobes usually gets larger in comparison to the maximum amplitude of the image, resulting in a less well defined central maximum and worse location accuracy.

Fig. 1b shows a vertical slice through the volume image, with the slice indicated by the dashed black line in Fig. 1a. The high-intensity area of the volume image is much more dispersed in the vertical than it is in the horizontal. This happens because the CAMMA is deployed in an approximately planar array with relatively small variations in the altitude of the sensors. The effect on the final location of the source is higher location uncertainty in the vertical than in the horizontal, and is a fundamental feature of all planar lightning locating systems (Thomas et al., 2004).

Fig. 1c shows the signals recorded from each sensor for the imaged 750-μs window. The waveforms from each sensor have been aligned by subtracting off the time-delay from the sensor location to the location of the brightest voxel in Figs. 1a and 1b. Because of the long duration of the window, multiple pulses can be seen in the signals from each sensor. The largest of these pulses happens about 550 μs in the window.

In order to locate each of the pulses, the aligned 750-μs windows were partitioned into 25 30-μs sub-windows. The sub-window numbers are labeled at the top of Fig. 1c. Similar to what has been done for the

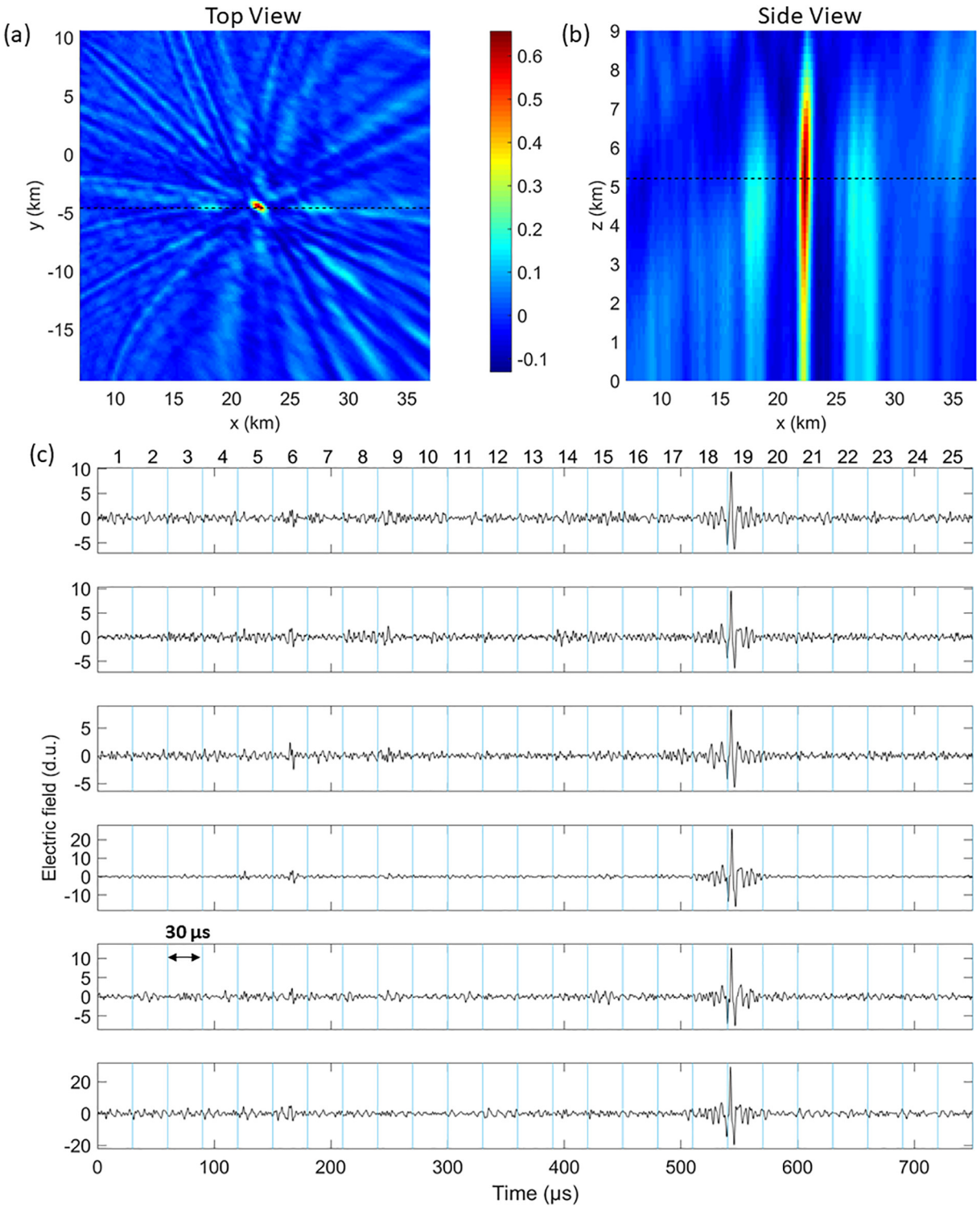

Fig. 1. (a) and (b) The sliced views of the normalized total correlations of 750-µs electric field waveforms from 6 stations. The slices were taken at the source location (brightest voxel), which are indicated by the black dashed lines. (c) The aligned 750-µs waveforms after 100–500 kHz band-pass filtering.

750-µs big window, the cross-correlation is performed again for each 30-µs sub-window and the total correlations were computed within a smaller computation volume, which is a cube centered at the source location determined from the 750-µs window with a side length of 6 km (± 3 km of the 750-µs-window source location). A smaller grid size of 50 m is used in the small computation volume to boost location accuracy. We used a smaller volume to image the source because the waveform was roughly aligned through the cross-correlations of the 750-µs windows and only small further alignment is needed through the cross-correlation of the sub-windows. Fig. 2 shows the top views of the normalized total correlations of the 25 30-µs windows in Fig. 1c with each panel corresponding to a sub-window. The brightest pixel in each panel is marked by a cross. The maximum normalized total correlation value of each panel is given at the lower-left corner. To distinguish between images produced by noise and images of a lightning source, we apply a simple threshold on the maximum total correlation value. This

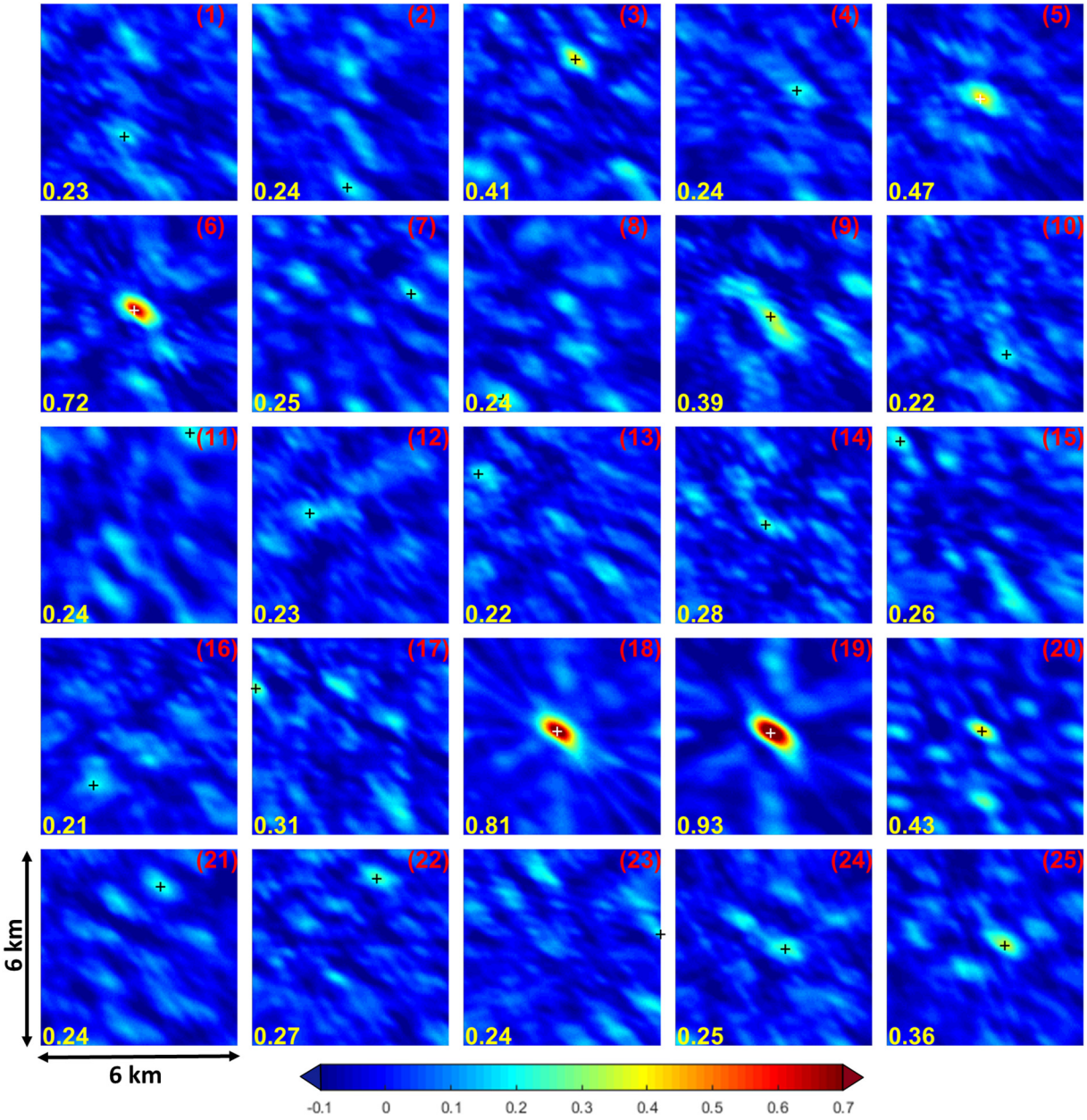

Fig. 2. The top view of the normalized total correlations of the 25 30-μs windows in Fig. 1c. The window number is given at the upper right corner of each panel. The brightest pixels are marked with crosses (white ones for lightning sources and black ones for noises) and its corresponding maximum total correlation value is given at the lower-left corner of each panel. Windows 5, 6, 18, and 19 contain lightning sources with a threshold of 0.45 on the maximum total correlation.

correlation threshold works in a similar way to the chi-square threshold used in the TOA-based algorithm. Using a threshold of 0.45, a total of four lightning sources marked by white crosses in Fig. 2 were identified out of the 25 sub-windows. Explanations of the selection of 0.45 can be found in Section 3.1. Three bright sources can be seen for windows 6, 18 and 19 and one faint source can be seen in window 5, which have amplitudes exceeding this threshold. The imaging process was repeated for each of the 750-μs windows and sources with maximum total correlation above the threshold were added to form a lightning map.

In the imaging algorithm, a 3D imaging volume (domain) that contains lightning sources has to be specified to apply the steps stated above. The area covered by the CAMMA is about 150 km by 150 km. For flashes further away from the area, high-quality maps usually cannot be produced. Without knowing where a flash is, imaging the entire 150*150 km domain with 200 m resolution (for big window) is computationally expensive and unnecessary. Instead, we can image the entire domain (150 km by 150 km by 20 km) with 1-km resolution (or larger with the inclusion of lower-frequency components) with waveforms from each big-window (750-μs) only to find out roughly where the flash is. With rough flash locations, we can determine the volume for further imaging with better resolution.

The frequency content of the waveform affects the image and location of the lightning source. To illustrate this, digital band-pass filters were applied to waveforms with passbands of 100–500 kHz (also used for Figs. 1 and 2), 50–150 kHz, and 300–500 kHz. The images using 30-μs electric field waveforms of different frequency content are shown in Fig. 3. Although the images of different frequency vary, the source locations (marked by the white crosses) are within 100 m of each other in X and Y, and within 400 m in height. In general, as the center frequency of the band goes higher, the size of the global maxima of the image gets smaller, and as the fractional bandwidth goes lower, the amplitude of the side lobes of the image becomes larger in comparison to the global

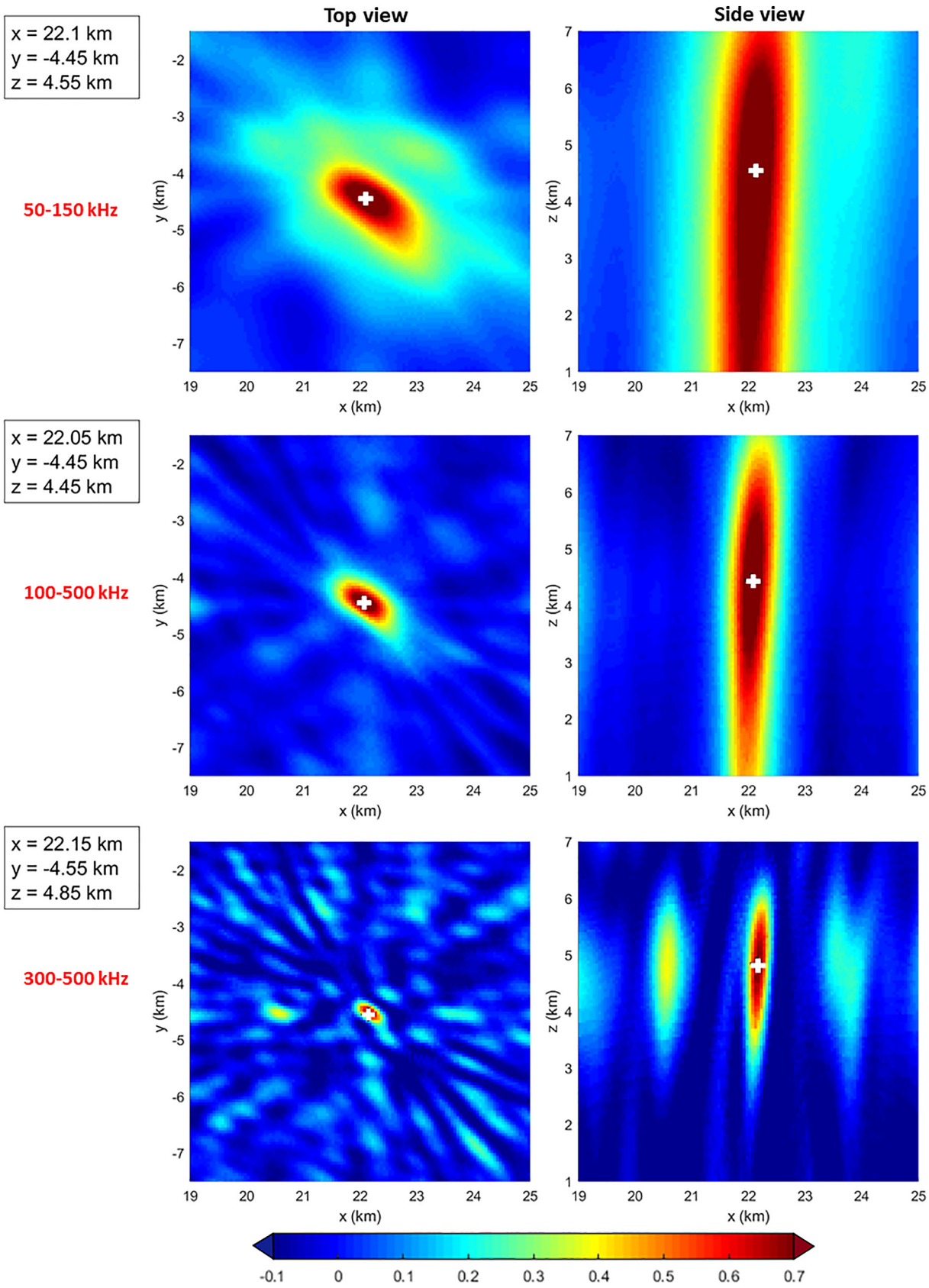

Fig. 3. The correlation image produced by 30-μs electric field waveforms (corresponding to sub-window 18 in Fig. 1) of different frequency contents. The source locations are marked by white crosses and the coordinates are given at the left side of this figure.

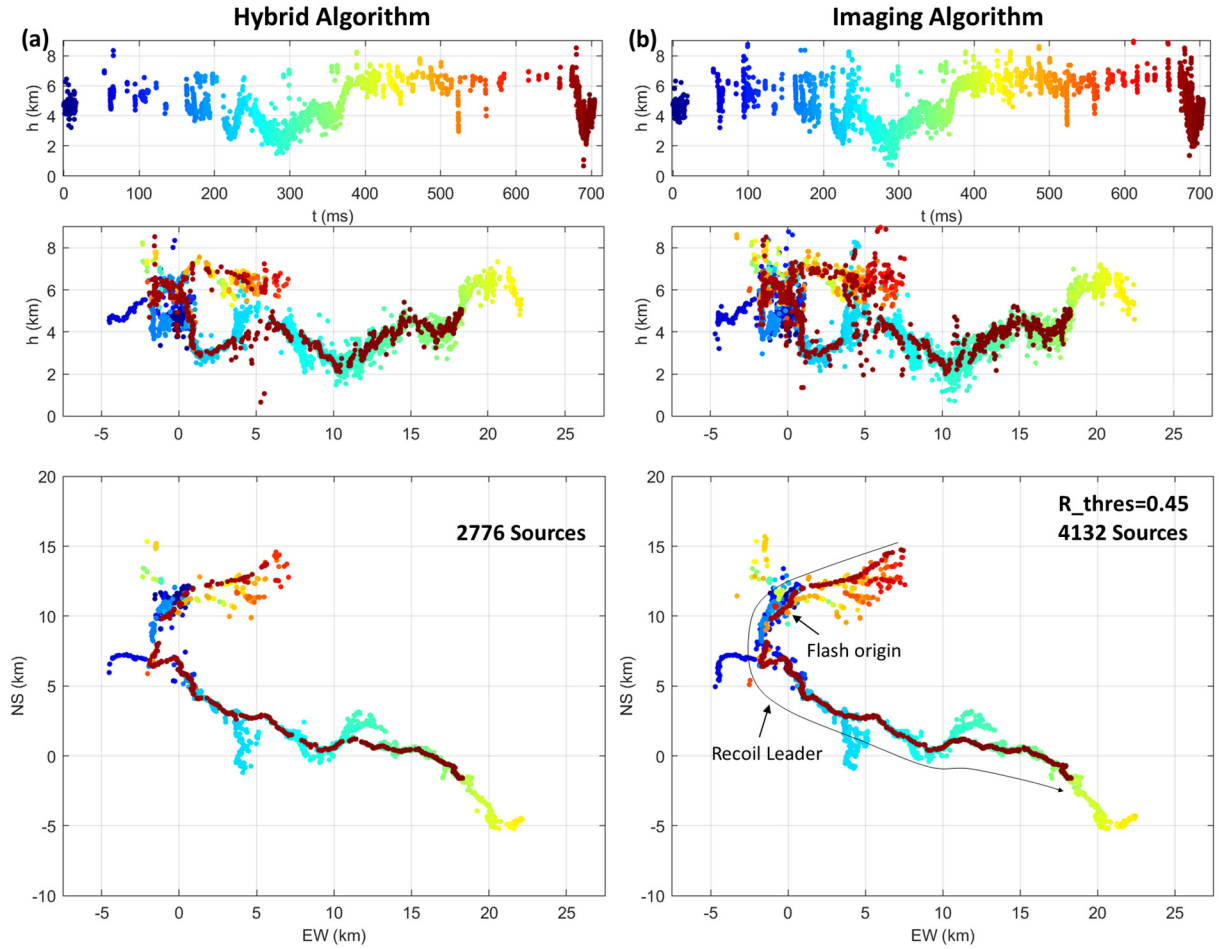

Fig. 4. The comparison of the lightning maps produced by the hybrid interferometric-TOA algorithm (left) and the imaging algorithm (right) with the threshold for maximum correlation being set as 0.45 for the imaging algorithm.

maxima.

3. Results

3.1. An inverted intracloud flash mapped by imaging algorithm

An inverted intracloud flash mapped by the imaging algorithm is shown in Fig. 4b. This flash initiated at a height of 4.8 km (the flash origin is marked in Fig. 4b) and propagated bi-directionally, although the inferred positive leader that moved towards the northeast appears to be not very active. In contrast, the negative leader was moving continuously at a lower altitude towards the southeast. Near the end of the flash, a faster recoil negative leader initiated at the tip of the remnants of the positive leader and traversed the channel. The recoil leader passed through the flash origin and continued propagating along three-quarters of the main negative leader channel. More information on this flash can be found in Zhu et al. (2020).

There is a tradeoff between the sensitivity (the capability to detect more lightning sources) and the reliability of the source location in choosing the threshold. A higher correlation threshold produces a map with more reliable source locations, but with less sensitivity and a smaller number of sources. Conversely, a lower threshold locates more sources but causes more noise solutions to be present in the map. There is a similar effect in the TOA-based algorithms with chi-squared value; accepting higher chi-squared gives more sources, but with worse accuracy. For this flash, a threshold of 0.45 is chosen for the purpose of removing most of the apparent noises and keeping the details of lightning channel structures at the same time. Maps of the same flash using different thresholds ranging from 0.3 to 0.75 can be found in Fig. 5. With the threshold of maximum correlation being set to 0.3 in Fig. 5a, a considerable number of noise sources are added to the map of the lightning flash. Most of the apparent noises are removed after the threshold increased to 0.45 in Fig. 5b. The number of sources in the map continues to decrease if we further increase the threshold, as shown in Fig. 5c and d. In Fig. 5d, the trunk of lightning channels is kept, but some portions of the map are now missing. For example, the fast recoil leader appears to be intermittent in Fig. 5d but we can tell from Fig. 5b that it propagated continuously. Also, the branching structure of the positive leaders in the northern end of the flash is almost indiscernible in Fig. 5d. The use of maximum total correlation is a simple way to discriminate between lightning source and noise but it has room to improve. A better lightning source/noise discrimination method that utilizes more parameters other than just the maximum total correlation is desired in the future.

Fig. 4a shows the lightning map produced by the hybrid interferometric-TOA algorithm used in Zhu et al. (2020) in comparison to that produced by the imaging algorithm in Fig. 4b. As expected, the overall flash structures produced by the two algorithms look very similar. The imaging algorithm located approximately 50% more sources than that of the hybrid algorithm, and the imaging algorithm produced a finer branched structure of the positive leaders. Note that the window sizes (for both big and sub-windows) used in the two algorithms are the same. Also, the imaging algorithm depicted continuous propagation in the first several milliseconds of the recoil leader (dark red sources in Fig. 4), which was not completely mapped by the hybrid algorithm. However, the heights of lightning sources obtained from the imaging

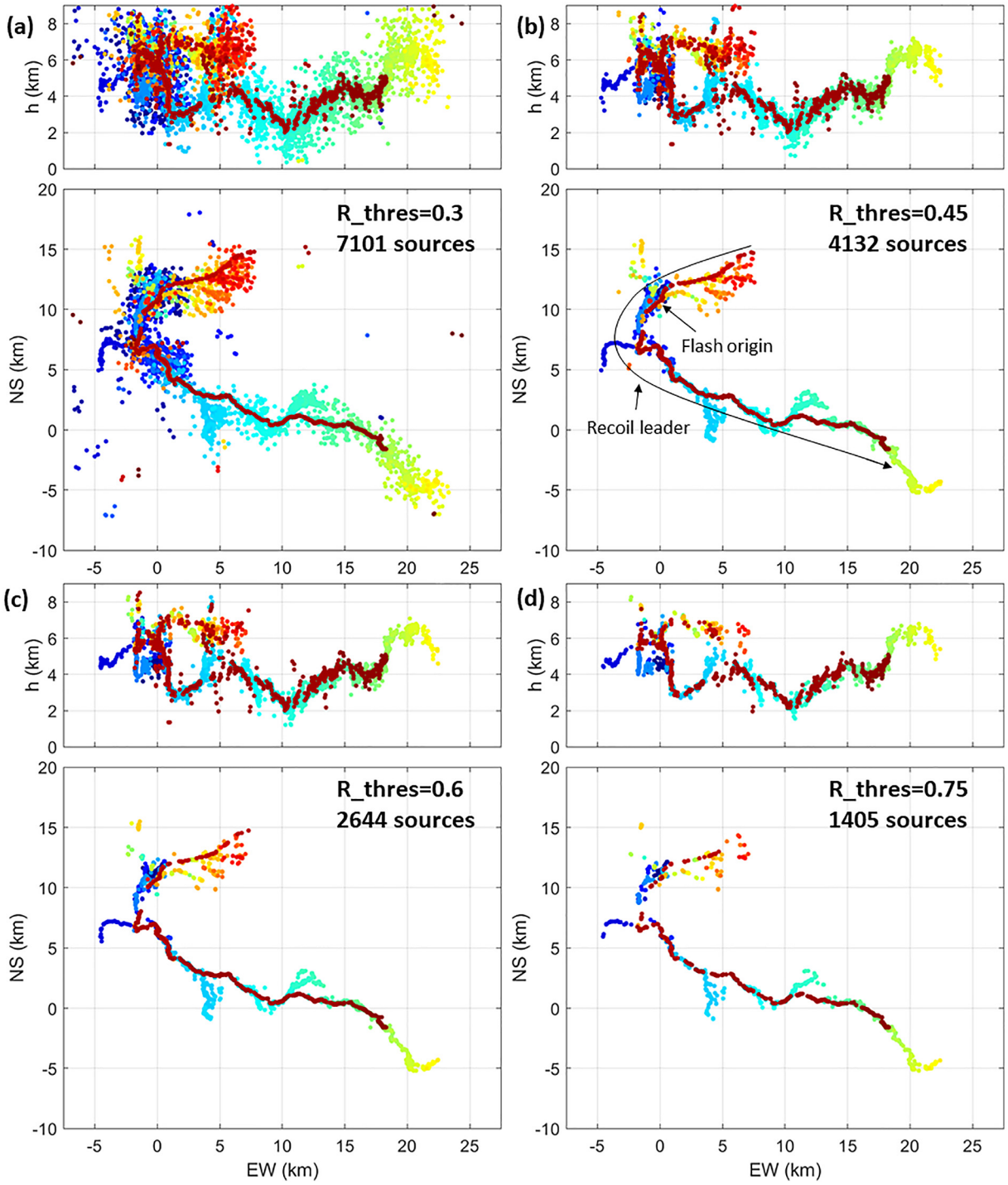

Fig. 5. Maps of the intracloud lightning flash produced by the imaging location algorithm, using different thresholds on the maximum correlation to filter out noise.

algorithm are more dispersive, suggesting a larger location error in height. Additional maps of lightning flashes comparing the results of the two algorithms can be found in Figs. S1 and S2 in the supplementary material.

Overall, the sensitivity of the imaging algorithm is higher than that of the hybrid-TOA algorithm. One reason for this is that the imaging algorithm uses correlations between all pairs of antennas (N(N-1)/2 correlations), while the hybrid-TOA algorithm correlates all antennas to a single "master" antenna (N -1 correlations). Another reason is that in the hybrid algorithm, a single correlation peak is chosen for the time difference, and if the wrong correlation peak is chosen then the time difference will be in error and the chi-squared of the solution will increase greatly; in contrast, the imaging algorithm automatically considers all peaks of the correlation while computing the image. This strength becomes more noticeable as the number of stations increases. With enough antennas, sources can be located even when many of the antenna pairs have poor correlations. This strength also enables the imaging algorithm to locate multiple simultaneously radiating sources.

The current form of imaging algorithm is more computationally expensive than the hybrid algorithm, and it becomes even more computationally expensive with increasing number of stations, larger imaging volume, and finer resolution. The portion of the imaging algorithm that requires intensive computation has already been put into GPU arrays to boost the computation speed. With a decent desktop equipped

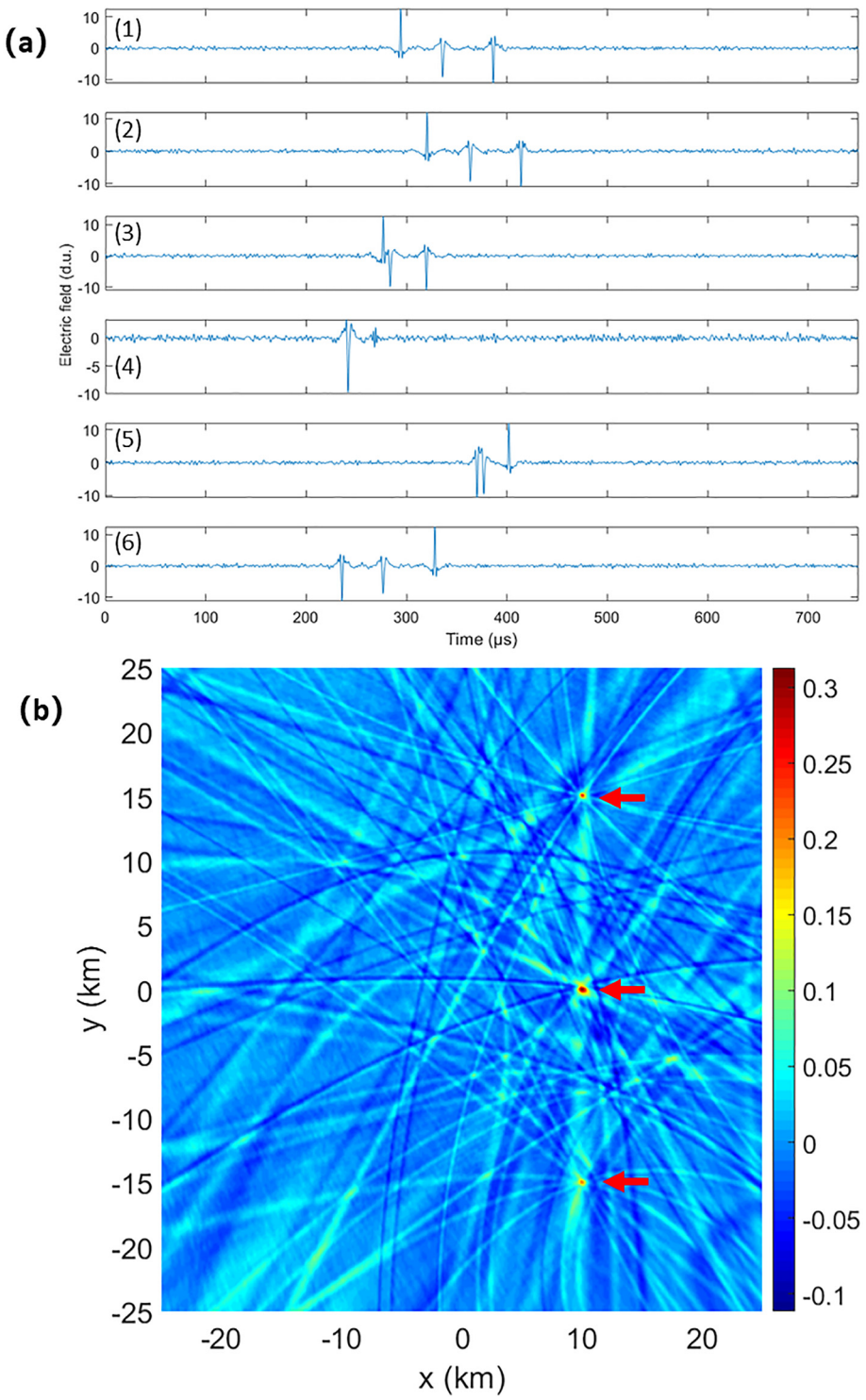

Fig. 6. (a) Simulated 750-μs electric field waveforms emitted by three lightning sources (at the same altitude) at six CAMMA stations. (b) The top view of the total correlations using the waveforms in Fig. 6a. Three sources are marked by red arrows.

with the intel i7-9700k processor and NVIDIA GeForce RTX 2070 graphics card (for GPU computing), it took the imaging algorithm 10 min to map the entire flash presented in Fig. 4 vs. 2 min or so for the hybrid algorithm. If we increase the voxel size by a factor of 2, the computation time will decrease by a factor of 8. In the future, we plan to further optimize the imaging algorithm to make it run faster.

3.2. Multiple concurrent sources imaging

One potential strength of the imaging algorithm is that it can locate multiple concurrent lightning sources, something that is very difficult to do with a TOA-based algorithm. A simulation has been developed to showcase this capability and illustrate its limitations. For this simulation, we chose three different lightning pulses from CAMMA records and used them as the emitted electric field for three concurrent lightning point sources. The three lightning sources were all placed at the

same height and all emitted at the same time, but were separated in the north-south direction by 15 km. The electric field was then propagated to six CAMMA stations (same as the CAMMA configuration in Argentina when the flash presented in Fig. 4 was recorded). Finally, the simulated electric field waveforms at all stations were superimposed with white noise. The simulated electric field waveforms were then passed through the imaging algorithm as normal, utilizing a 100–500 kHz band-pass filter. The filtered 750-μs electric field waveforms are shown in Fig. 6a. It can be seen that the individual pulses are well separated by tens of microseconds from each other in sub-panels 1,2,6, but are very close or even superimposed in sub-panels 3,4,5. Also, the three pulses appear in different orders for some stations (e.g. stations 1 and 6). This would make it very difficult for a traditional TOA-based algorithm to identify matched peaks for locating, especially when the separation between pulses is smaller than the length of the pulse-searching window used in the TOA algorithm. The resulting image of the simulated waveforms is shown in Fig. 6b, with all three sources clearly seen. The image is not without limitations though, the background noise in Fig. 6b is substantially higher than that seen in Fig. 1a. As additional sources are added, the background noise will continue to increase until the point sources cannot be distinguished. Conversely, using more antennas will reduce the background noise and allow more concurrent point sources to be located. Also, the image is limited by the resolution of the array. If the sources are too close together, they will merge into a single source in the image.

4. Summary

The imaging algorithm, a purely interferometric lightning location algorithm that can be used in low-frequency lightning mapping, was presented in this paper. Unlike traditional TOA-based location algorithms that send the arrival times or arrival time differences into a non-linear minimizer to determine the location of the source, the imaging algorithm determines the location of a lightning source by computing the three-dimensional total correlation of lightning signals at different stations and finding the location where the total correlation is largest. As an example, the map for an intracloud flash with a long recoil leader was produced by the imaging algorithm and the map was compared with that of the hybrid interferometric-TOA algorithm. It was found that the imaging algorithm was able to locate about 50% more sources than the hybrid algorithm. We also simulated a scenario in which three lightning sources separated by 15 km emitted electric field at the same time. The three concurrent lightning sources can be located by imaging the simulated lightning signals at six stations. This simulation demonstrated that the imaging algorithm is potentially capable of locating multiple concurrent lightning sources even when some pulses are merged, which is very difficult for the traditional TOA-based technique.

There is still plenty of room for improvement in the imaging algorithm which we expect will make it even better in the future. It is possible in Fig. 2 that the current source/signal discrimination technique is omitting some real sources. In the future, we hope that a multi-parameter discrimination technique could increase the number of sources located while still rejecting noise-contaminated solutions. Additionally, the current imaging algorithm is more computationally expensive than TOA-based algorithms. More optimization is desired to make the imaging algorithm to run faster in the future. It may also be possible to combine the strengths of the imaging algorithm with other location techniques to, for example, improve source height accuracy.

Declaration of Competing Interest

None.

Acknowledgment

This research was supported by U.S. National Science Foundation grants AGS-1654576 and AGS- 1661785. The authors thank Jeff Burchfield, Lawrence Carey, Bruno Medina, Jacquelyn Ringhausen, Lena Heuscher for operating the array in the field campaign.

Author statement

M. Stock and Y. Zhu conceived the idea for this study. Y. Zhu developed the processing code. Y. Zhu and M. Stock drafted the manuscript. P. Bitzer led the instrument development and obtained the data for this study. All authors contributed to the discussion of the results and preparation of the manuscript.

Declaration of Competing Interest

The authors declare that they have no known competing financial interests or personal relationships that could have appeared to influence the work reported in this paper.

Appendix A. Supplementary data

Supplementary data to this article can be found online at https://doi.org/10.1016/j.atmosres.2020.105139.

References

Bitzer, P.M., Christian, H.J., Stewart, M., Burchfield, J., Podgorny, S., Corredor, D., et al., 2013. Characterization and applications of VLF/LF source locations from lightning using the Huntsville Alabama Marx Meter Array. J. Geophys. Res.-Atmos. 118 (8), 3120–3138. https://doi.org/10.1002/jgrd.50271.

Cummins, K.L., Murphy, M.J., 2009. An overview of lightning locating systems: History, techniques, and data uses, with an in-depth look at the U.S. NLDN. IEEE Trans. Electromagn. Compat. 51 (3 PART 1), 499–518. https://doi.org/10.1109/TEMC.2009.2023450.

Cummins, K.L., Murphy, M.J., Bardo, E.A., Hiscox, W.L., Pyle, R.B., Pifer, A.E., 1998. A combined TOA/MDF Technology Upgrade of the U.S. National Lightning Detection Network. J. Geophys. Res. 103 (D8), 9035. https://doi.org/10.1029/98JD00153.

Hare, B.M., Scholten, O., Dwyer, J., Ebert, U., Nijdam, S., Bonardi, A., et al., 2020. Radio Emission reveals Inner Meter-Scale Structure of negative Lightning Leader steps. Phys. Rev. Lett. 124 (10), 105101. https://doi.org/10.1103/PhysRevLett.124.105101.

Karunarathne, S., Marshall, T.C., Stolzenburg, M., Karunarathna, N., Vickers, L.E., Warner, T.A., Orville, R.E., 2013. Locating initial breakdown pulses using electric field change network. J. Geophys. Res.-Atmos. 118 (13), 7129–7141. https://doi.org/10.1002/jgrd.50441.

Lang, T.J., Pédeboy, S., Rison, W., Cerveny, R.S., Montanyà, J., Chauzy, S., et al., 2017. WMO World Record Lightning Extremes: Longest Reported Flash Distance and Longest Reported Flash Duration. Bull. Am. Meteorol. Soc. 98 (6), 1153–1168. https://doi.org/10.1175/BAMS-D-16-0061.1.

Lyu, F., Cummer, S.A., Solanki, R., Weinert, J., McTague, L., Katko, A., et al., 2014. A low-frequency near-field interferometric-TOA 3-D Lightning Mapping Array. Geophys. Res. Lett. 41 (22), 7777–7784. https://doi.org/10.1002/2014GL061963.

Rison, W., Thomas, R.J., Krehbiel, P.R., Hamlin, T., Harlin, J., 1999. A GPS-based three-dimensional lightning mapping system: initial observations in Central New Mexico. Geophys. Res. Lett. 26 (23), 3573–3576. https://doi.org/10.1029/1999GL010856.

Shao, X.-M., Stanley, M., Regan, A., Harlin, J., Pongratz, M., Stock, M., 2006. Total Lightning Observations with the New and improved Los Alamos Sferic Array (LASA). J. Atmos. Ocean. Technol. 23 (10), 1273–1288. https://doi.org/10.1175/JTECH1908.1.

Shi, D.D., Zheng, D., Zhang, Y., Zhang, Y.J., Huang, Z.G., Lu, W.T., et al., 2017. Low-frequency E-field Detection Array (LFEDA)—Construction and preliminary results. Sci. China Earth Sci. 60 (10), 1896–1908. https://doi.org/10.1007/s11430-016-9093-9.

Shi, F., Liu, N., Dwyer, J.R., Ihaddadene, K.M.A., 2019. VHF and UHF Electromagnetic Radiation Produced by Streamers in Lightning. Geophys. Res. Lett. 46 (1), 443–451. https://doi.org/10.1029/2018GL080309.

Stock, M., Krehbiel, P., 2014. Multiple baseline lightning interferometry - improving the detection of low amplitude VHF sources. In: 2014 International Conference on Lightning Protection (ICLP). IEEE, pp. 293–300. https://doi.org/10.1109/ICLP.2014.6973139.

Stock, M.G., Akita, M., Krehbiel, P.R., Rison, W., Edens, H.E., Kawasaki, Z., Stanley, M.A., 2014. Continuous broadband digital interferometry of lightning using a generalized cross-correlation algorithm. J. Geophys. Res.-Atmos. 119 (6), 3134–3165. https://doi.org/10.1002/2013JD020217.

Stock, M., Wu, T., Akiyama, Y., Ushio, T., Kawasaki, Z., Nakamura, Y., et al., 2016.

Improvements to the BOLT lightning location system. In: 2016 33rd International Conference on Lightning Protection (ICLP). IEEE, pp. 1–4. https://doi.org/10.1109/ICLP.2016.7791365.

Sun, Z., Qie, X., Liu, M., Cao, D., Wang, D., 2013. Lightning VHF radiation location system based on short-baseline TDOA technique - Validation in rocket-triggered lightning. Atmos. Res. 129–130. 58–66. https://doi.org/10.1016/j.atmosres.2012.11.010.

Thomas, R.J., Krehbiel, P.R., Rison, W., Hunyady, S.J., Winn, W.P., Hamlin, T., Harlin, J., 2004. Accuracy of the lightning mapping array. Journal of Geophysical Research D: Atmospheres 109 (14), 1–34. https://doi.org/10.1029/2004JD004549.

Wang, Y., Qie, X., Wang, D., Liu, M., Su, D., Wang, Z., et al., 2016. Beijing Lightning Network (BLNET) and the observation on preliminary breakdown processes. Atmos. Res. 171, 121–132. https://doi.org/10.1016/j.atmosres.2015.12.012.

Wang, T., Shi, L., Qiu, S., Sun, Z., Duan, Y., 2020. Continuous broadband lightning VHF mapping array using MUSIC algorithm. Atmos. Res. 231, 104647. https://doi.org/10.1016/j.atmosres.2019.104647.

Wu, T., Wang, D., Takagi, N., 2018. Lightning Mapping with an Array of Fast Antennas. Geophys. Res. Lett. 45 (8), 3698–3705. https://doi.org/10.1002/2018GL077628.

Wu, T., Wang, D., Takagi, N., 2019. Velocities of positive Leaders in Intracloud and negative Cloud-to-Ground Lightning Flashes. J. Geophys. Res.-Atmos. 124 (17–18), 9983–9995. https://doi.org/10.1029/2019JD030783.

Yoshida, S., Wu, T., Ushio, T., Kusunoki, K., Nakamura, Y., 2014. Initial results of LF sensor network for lightning observation and characteristics of lightning emission in LF band. J. Geophys. Res.-Atmos. 119 (21), 12,034–12,051. https://doi.org/10.1002/2014JD022065.

Zhu, Y., Rakov, V.A., Tran, M.D., Stock, M.G., Heckman, S., Liu, C., et al., 2017. Evaluation of ENTLN Performance Characteristics based on the Ground Truth Natural and Rocket-Triggered Lightning Data acquired in Florida. J. Geophys. Res.-Atmos. https://doi.org/10.1002/2017JD027270.

Zhu, Y., Bitzer, P., Stewart, M., Podgorny, S., Corredor, D., Burchfield, J., et al., 2020. Huntsville Alabama Marx Meter Array 2: Upgrade and Capability. Earth and Space Science 7 (4), e2020EA001111. https://doi.org/10.1029/2020EA001111.